![White Rose university consortium logo - Universities of Leeds, Sheffield & York]

eprints@whiterose.ac.uk
https://eprints.whiterose.ac.uk/

The Speciation of Homochiral and Heterochiral Diastereomers of Homoleptic Cobalt(II) and Zinc(II) PyBox Complexes

Kay E. Burrows,[a]* Rafal Kulmaczewski,[a] Oscar Cespedes,[b] Simon A. Barrett[a] and Malcolm A. Halcrow[a]*

[a] School of Chemistry, University of Leeds, Woodhouse Lane, Leeds,LS2 9JT (UK). E-mail: m.a.halcrow@leeds.ac.uk

[b] School of Physics and Astronomy, University of Leeds, Woodhouse Lane, Leeds, LS2 9JT (UK)

Abstract

Homochiral $[M((R)-L^R)_2]^{2+}$ and heterochiral $[M((R)-L^R)((S)-L^R)]^{2+}$ isomers of $[Zn(L^{Ph})_2][BF_4]_2$, $[Zn(L^{iPr})_2][BF_4]_2$, $[Co(L^{Ph})_2][BF_4]_2$, and $[Co(L^{iPr})_2][BF_4]_2$ (L^{Ph} = 2,6-*bis*(4-phenyloxazolinyl)pyridine; L^{iPr} = 2,6-*bis*(4-*iso*propyloxazolinyl)pyridine) have been prepared and characterised. Six of the eight compounds were crystallographically characterised, showing that steric repulsions between ligand substituents lead to more distorted coordination geometries in the homochiral isomers, especially in the L^{iPr} complexes. Heterochiral $[M((R)-L^{iPr})((S)-L^{iPr})]^{2+}$ (M = Zn or Co) undergoes partial racemisation in CD_3CN through ligand redistribution reactions, whereas $[M((R)-L^{Ph})((S)-L^{Ph})]^{2+}$ does not (in agreement with previous reports). This may be a consequence of intramolecular $\pi...\pi$-interactions in $[M((R)-L^{Ph})((S)-L^{Ph})]^{2+}$, whereby each pyridyl group is sandwiched between two phenyl substituents from the other L^{Ph} ligand. These $\pi...\pi$-interactions are disrupted in homochiral $[M((R)-L^R)_2]^{2+}$, owing to the aforementioned steric clash between phenyl substituents in that isomer.

Dedicated to Spyros Perlepes on the occasion of his 65th birthday.

1. Introduction

2,6-*Bis*(oxazolinyl)pyridine (PyBox) derivatives (Scheme 1) are readily available in optically pure form [1], and are well established as tridentate supporting ligands in asymmetric catalysis [2]. More recently, their chirality has also been exploited in other aspects of coordination chemistry including molecular magnetism [3], supramolecular chemistry [4] and spin-crossover complexes [5, 6]. During our continued studies of spin-crossover compounds based on tridentate diazolylpyridine derivatives [7], we recently demonstrated an unambiguous influence of chirality on molecular spin state, through solution measurements on diastereomers of $[Fe(L^{Ph})_2][ClO_4]_2$ (Scheme 1) [8]. That is, homochiral (*rac*) $[Fe((R)-L^{Ph})_2][ClO_4]_2$ undergoes spin-crossover at 34 K lower temperature than heterochiral (*meso*) $[Fe((R)-L^{Ph})((S)-L^{Ph})][ClO_4]_2$ in CD_3CN solution [6]. We attributed this to a more twisted coordination geometry adopted by the homochiral isomer, caused by an inter-ligand steric clash between phenyl substituents, which stabilises the more plastic high-spin form of that isomer to a small degree.

<Insert Scheme 1 here>

That study was possible, because heterochiral $[Fe((R)-L^{Ph})((S)-L^{Ph})][ClO_4]_2$ is stable in solution, and does not undergo detectable racemisation through ligand redistribution [9]. The same is true for salts of the analogous complexes $[M((R)-L^{Ph})((S)-L^{Ph})]^{2+}$ (M = Co [10, 11], Zn [12], Cu [13] or another metal ion [9]). However, in contrast, heterochiral $[Fe((R)-L^{iPr})((S)-L^{iPr})][ClO_4]_2$ [6], and $[Co((R)-L^R)((S)-L^R)]^{2+}$ (R = Me or Bn) [10], do undergo partial racemisation under the same conditions. Hence, the solution stability of heterochiral $[M(PyBox)_2]^{2+}$ derivatives appears to depend on the PyBox 'R' substituents (Scheme 1). To probe this further, we report here a comparison of homochiral and heterochiral $[Co(L^{Ph})_2]^{2+}$ [10, 11] and $[Zn(L^{Ph})_2]^{2+}$ [12] with the (previously unreported) diastereomers of $[Co(L^{iPr})_2]^{2+}$ and $[Zn(L^{iPr})_2]^{2+}$.

2. Experimental

Instrumentation

^{1}H NMR spectra were obtained using a Bruker DPX300 or Avance 500 FT spectrometer, operating at 300.2 and 500.1 MHz respectively. Mass spectrometry was performed using a Bruker Daltonics (micro T.O.F) instrument operating in the positive ion electrospray mode. All spectra were recorded using acetonitrile as eluent and sodium formate solution to calibrate the system. Solid state magnetic susceptibility measurements were performed using a Quantum Design SQUID/VSM magnetometer in an applied field of 5000 G and a temperature ramp of 5 Kmin^{-1}. Diamagnetic corrections for the samples were estimated from Pascal's constants [14]; a previously measured diamagnetic correction for the sample holder was also applied to the data. Evans method magnetic susceptibility measurements in solution were performed on a Bruker Avance 500 FT NMR spectrometer operating at 500.1 MHz, using tetramethylsilane as a reference [15]. A diamagnetic correction for the sample

[14] and a correction for the variation of the density of the CD_3CN solvent with temperature [16] were applied to these data.

Materials and methods

2,6-*Bis*(4-(*R*)-phenyloxazolinyl)pyridine ((*R*)-*L*^Ph), 2,6-*bis*(4-(*S*)-phenyloxazolinyl)pyridine ((*S*)-*L*^Ph), 2,6-*bis*(4-(*R*)-*iso*propyloxazolinyl)pyridine ((*R*)-*L*^iPr), 2,6-*bis*(4-(*S*)-*iso*propyloxazolinyl)pyridine ((*S*)-*L*^iPr) and all metal salts and solvents were purchased commercially and used as supplied.

Synthesis of [Zn((*R*)-*L*^Ph)$_2$][BF$_4$]$_2$ ((*R*)-1)

Zinc(II) tetrafluoroborate hydrate (16 mg, 0.068 mmol) was added to a solution of (*R*)-*L*^Ph (50 mg, 0.135 mmol) in acetonitrile (15 cm^3). The resultant colourless solution was stirred at room temperature for one hour, before the product was precipitated using excess diethyl ether. The white precipitate was collected using vacuum filtration. Single crystals suitable for X-ray diffraction analysis were grown by vapour diffusion of diethyl ether into a concentrated solution of the product in acetonitrile. Yield: 0.056 g, 84%. Elemental microanalysis: found C 56.7, H 3.38, N 8.99 %: calcd for $C_{46}H_{38}B_2F_8N_6O_4Zn$ C 56.5, H 3.92, N 8.59 %. ^{1}H NMR (CD$_3$CN): δ 4.75 (dd, 4H, 10.8, 8,9 Hz, C*H*), 5.23 (dd, 4H, 10.4, 8.9 Hz, ox-*H*), 5.15 (t, 4H, 10.6 Hz, ox-*H*), 6.76 (d, 8H, 7.2 Hz, Ph *H*^2/6), 7.09 (t, 8H, 7.2 Hz, Ph *H*^3/5), 7.22 (m, 4H, Ph *H*^4), 8.04 (d, 4H, 7.9 Hz, Py *H*^3/5), 8.47 (t, 2H, 7.9 Hz, Py *H*^4).

Synthesis of [Zn((*R*)-*L*^Ph)((*S*)-*L*^Ph)][BF$_4$]$_2$ ((*RS*)-1)

Method as for (*R*)-**1**, but using a mixture of (*R*)-*L*^Ph (25 mg, 0.068 mmol), and (*S*)-*L*^Ph (25 mg, 0.068 mmol). The product was crystallised by vapour diffusion from acetonitrile/diethyl ether Yield: 0.06 g, 90 %. Elemental microanalysis: found C 56.5, H 3.79, N 8.54 %: calcd for $C_{46}H_{38}B_2F_8N_6O_4Zn$ C 56.5, H 3.92, N 8.59 %. ^{1}H NMR (CD$_3$CN): δ 4.69 (dd, 4H, 10.4, 9.0 Hz, C*H*), 4.79 (t, 4H, 9.2 Hz, ox-*H*), 4.99 (dd, 4H, 10.4, 9.5 Hz, ox-*H*), 6.93 (d, 8H, 8.2 Hz, Ph *H*^2/6), 7.16 (t, 8H, 7.2 Hz, Ph *H*^3/5), 7.23-7.27 (m, 4H, Ph *H*^4), 7.99 (d, 4H, 7.9 Hz, Py *H*^3/5), 8.46 (t, 2H, 7.9 Hz, Py *H*^4).

Synthesis of [Zn((*R*)-*L*^iPr)$_2$][BF$_4$]$_2$ ((*R*)-2)

(*R*)-*L*^iPr (50 mg, 0.17 mmol) was dissolved in acetonitrile (15 cm^3). Zinc(II) tetrafluoroborate hydrate (20 mg, 0.083 mmol) was then added and the solution stirred at room temperature for one hour. A large excess of diethyl ether was added and the resultant precipitate was isolated by vacuum filtration leaving a white powder. Single crystals suitable for X-ray diffraction analysis were grown by vapour diffusion of diethyl ether into a concentrated solution of the product in acetonitrile. Yield: 0.054 g, 78%. Elemental microanalysis: found C 48.4, H 5.39, N 10.0 %: calcd for $C_{34}H_{46}B_2F_8N_6O_4Zn$ C 48.5, H 5.51, N 9.98 %. ^{1}H NMR

(CD$_3$CN): δ 0.52 (d, 12H, 6.7 Hz, iPr CH_3), 0.64 (d, 12H, 6.7 Hz, iPr CH_3), 1.40 (dq, 4H, 13.4, 6.7 Hz, iPr CH), 3.89 (ddd, 4H, 10.0, 8.7, 6.6 Hz, ox-H), 4.67 (t, 4H, 8.9 Hz, ox-H), 4.97 (t, 4H, 9.7 Hz, ox-H), 8.41 (d, 4H, 7.9 Hz, Py $H^{3/5}$), 8.66 (t, 2H, 7.9 Hz, Py H^4).

Synthesis of [Zn((R)-L^{iPr})((S)-L^{Ph})][BF$_4$]$_2$ ((RS)-2)

Method as for (R)-**2**, but using a mixture of (R)-L^{iPr} (25 mg, 0.083 mmol) and (S)-L^{iPr} (25 mg, 0.083 mmol). The product was crystallised using an acetonitrile/diethyl ether vapour diffusion method. Yield: 0.06 g, 86 %. Elemental microanalysis: found C 48.4, H 5.43, N 10.0 %: calcd for C$_{34}$H$_{46}$B$_2$F$_8$N$_6$O$_4$Zn C 48.5, H 5.51, N 9.98 %. ^{1}H NMR (CD$_3$CN): δ 0.68 (d, 12H, 3.2 Hz, iPr CH_3), 0.69 (d, 12H, 3.2 Hz, iPr CH_3), 1.30 (qd, 4H, 10.7, 6.8 Hz, iPr CH), 4.14 (ddd, 4H, 7.8, 3.8 Hz, ox-H), 4.82-4.70 (m, 8H, ox-H), 8.38 (d, 4H, 7.9 Hz, Py $H^{3/5}$), 8.64 (t, 2H, 7.9 Hz, Py H^4).

Synthesis of [Co((R)-L^{Ph})$_2$][BF$_4$]$_2$ ((R)-3)

Cobalt(II) tetrafluoroborate hydrate (25 mg, 0.0675 mmol) was added to a solution of (R)-L^{Ph} (50 mg, 0.135 mmol) in acetonitrile (15 cm^3). The resultant orange solution was stirred at room temperature for one hour. The product was precipitated using an excess of diethyl ether and the precipitate was collected by vacuum filtration, leaving an orange powder. A vapour diffusion of diethyl ether into a concentrated solution of the complex in acetonitrile gave orange crystals suitable for X-ray diffraction. Yield: 0.056 g, 84%. Elemental microanalysis: found C 56.6, H 3.81, N 8.53 %: calcd for C$_{46}$H$_{38}$B$_2$CoF$_8$N$_6$O$_4$ C 56.9, H 3.94, N 8.65 %. ^{1}H NMR (CD$_3$CN): δ 2.7 (8H, Ph $H^{2/6}$), 3.0 (4H, Ph H^4), 7.7 (8H, Ph $H^{3/5}$), 20.0 and 36.8 (both 4H, Ox H^5), 40.5 (4H, Py $H^{3/5}$), 84.7 (4H, Ox H^4). No peak from the Py H^4 proton environment was observed, which may be obscured by the CHD$_2$CN solvent peak.

Synthesis of [Co((R)-L^{Ph})((S)-L^{Ph})][BF$_4$]$_2$ ((RS)-3)

Method as for (RS)-**1**, but using cobalt(II) tetrafluoroborate hydrate (25 mg, 0.0675 mmol). Single crystals suitable for X-ray diffraction analysis were grown by vapour diffusion of diethyl ether into a concentrated solution of the product in acetonitrile. Yield: 0.06 g, 90 %. Elemental microanalysis: found C 56.7, H 4.03, N 8.79 %: calcd for C$_{46}$H$_{38}$B$_2$CoF$_8$N$_6$O$_4$ C 56.9, H 3.94, N 8.65 %. ^{1}H NMR: (CD$_3$CN): δ 1.2 (2H, Py H^4), 7.3 (4H, Ph H^4), 8.0 (8H, Ph $H^{3/5}$), 16.2 (8H, Py $H^{2/6}$), 26.9 and 28.3 (both 4H, Ox H^5), 37.9 (4H, Py $H^{3/5}$), 72.4 (4H, Ox H^4).

Synthesis of [Co((R)-L^{iPr})$_2$][BF$_4$]$_2$ ((R)-4)

Method as for (RS)-**2**, using cobalt(II) tetrafluoroborate hydrate (20 mg, 0.0825 mmol).. Single crystals suitable for X-ray diffraction analysis were grown by vapour diffusion of diethyl ether into a concentrated solution of the orange complex in acetonitrile. Yield: 0.054 g, 78%. Elemental microanalysis: found C 49.0, H 5.40, N 10.1 %: calcd for C$_{34}$H$_{46}$B$_2$CoF$_8$N$_6$O$_4$

C 48.9, H 5.55, N 10.1 %. ^{1}H NMR (CD$_3$CN): δ −17.3 and −4.9 (both 12H, iPr CH$_3$), 9.0 (2H, Py H^4), 15.9 (4H, iPr CH), 26.2 and 26.8 (both 4H, Ox H^5), 54.6 (4H, Py H$^{3/5}$), 74.2 (4H, Ox H^4).

Synthesis of [Co((R)-L^{iPr})((S)-L^{iPr})][BF$_4$]$_2$ ((RS)-4)

Method as for (RS)-**2**, but using cobalt(II) tetrafluoroborate hydrate (20 mg, 0.0825 mmol). The product was crystallised using by vapour diffusion from acetonitrile/diethyl ether vapour diffusion. Yield: 0.06 g, 86 %. Elemental microanalysis: found C 48.7, H 5.65, N 9.98 %: calcd for C$_{34}$H$_{46}$B$_2$CoF$_8$N$_6$O$_4$ C 48.9, H 5.55, N 10.1 %. ^{1}H NMR (CD$_3$CN): δ 3.8 and 9.9 (both 12H, iPr CH$_3$), 10.0 (2H, 2H, Py H^4), 17.8 (4H, iPr CH), 21.7 and 30.4 (both 4H, Ox H^5), 45.2 (4H, Py H$^{3/5}$), 63.8 (4H, Ox H^4).

Single crystal X-ray structure determinations

All the single crystals in this work were grown by slow diffusion of diethyl ether vapour into acetonitrile solutions of the compounds. The diffraction data for (RS)-**4**·MeCN were recorded at station I19 of the Diamond synchrotron (λ = 0.6998 Å). All the other crystallographic data were measured with an Agilent Supernova dual-source diffractometer, using monochromated Cu-K$_\alpha$ (λ = 1.5418 Å). The diffractometer was fitted with an Oxford Cryostream low-temperature device. The structures were all solved by direct methods (*SHELXS97* [17]), and developed by full least-squares refinement on F^2 (*SHELXL97* [17]). Crystallographic figures were prepared using *OLEXII* [18]. Experimental details from these structure determinations are summarised in Table 1.

<Insert Table 1 here>

All non-H atoms in the structures were modelled anisotropically during the final least-squares refinement cycles, and H atoms were placed in calculated positions and refined using a riding model. Disordered BF$_4^-$ anions were modelled using refined B–F distance restraints, while disordered phenyl and *iso*propyl groups and solvent molecules were modelled using fixed bond distance restraints.

The asymmetric unit of (RS)-**1**·2.5MeCN contains four complex cations, eight BF$_4^-$ counterions and ten acetonitrile molecules. The structure was refined using the non-merohedral twin law (−1, 0, 0, 0, 1, 0, 0, 0, −1) with a domain ratio of 0.25(3). Disorder in two phenyl rings and two BF$_4^-$ ions was modelled as above. There are four residual Fourier peaks of 1.8-3.0 eÅ^{-3} in this refinement, each 0.8-1.0 Å from a zinc atom.

The asymmetric unit of (R)-**2**·0.5MeCN contains two complex cations, four tetrafluoroborate counterions and one acetonitrile molecule. No disorder is present in this refinement. All the other crystals contain one formula unit in their asymmetric unit. The structure containing the most disorder is (RS)-**4**·MeCN whose solvent is disordered within a cavity spanning the crystallographic inversion centre. Disorder in one *iso*-propyl group and one BF$_4^-$ anion was also included in that model. Two disordered phenyl rings in (RS)-**1**·3MeCN were also treated

with restraints as described above. No disorder was included in the other structure refinements.

3. Results and discussion

Treatment of hydrated $Zn[BF_4]_2$ with 2 equiv of $(R)\text{-}L^R$ (R = Ph or iPr; Scheme 1), or 1 equiv each of $(R)\text{-}L^R$ and $(S)\text{-}L^R$, in MeCN yielded the following colourless complexes after the usual work-up: $[Zn((R)\text{-}L^{Ph})_2][BF_4]_2$ ((R)-**1**), $[Zn((R)\text{-}L^{Ph})((S)\text{-}L^{Ph})][BF_4]_2$ ((RS)-**1**), $[Zn((R)\text{-}L^{iPr})_2][BF_4]_2$ ((R)-**2**) and $[Zn((R)\text{-}L^{iPr})((S)\text{-}L^{iPr})][BF_4]_2$ ((RS)-**2**). Analogous complexations using hydrated $Co[BF_4]_2$ gave the cobalt(II) analogues as orange polycrystalline solids: $[Co((R)\text{-}L^{Ph})_2][BF_4]_2$ ((R)-**3**); $[Co((R)\text{-}L^{Ph})((S)\text{-}L^{Ph})][BF_4]_2$ ((RS)-**3**), $[Co((R)\text{-}L^{iPr})_2][BF_4]_2$ ((R)-**4**) and $[Co((R)\text{-}L^{iPr})((S)\text{-}L^{iPr})][BF_4]_2$ ((RS)-**4**). While many of these compounds contained lattice solvent in their crystalline forms, microanalysis showed that all the complexes were obtained in their solvent-free forms after drying *in vacuo*. All four cobalt complexes are high-spin between 3-300 K in the solid state from magnetic susceptibility data, while (R)-**3** and (RS)-**3** are also fully high-spin in CD_3CN solution over the liquid range of the solvent (Figure 1). Hence, in contrast to their iron(II) analogues [6], the different diastereomers of **3** have identical spin state properties.

<Insert Figure 1 here>

Solvated or solvent-free single crystals of all the zinc complexes, (R)-**3** and (RS)-**4** were obtained by slow diffusion of diethyl ether into acetonitrile solutions of each compound. Crystals of (RS)-**1**·2.5MeCN adopt the monoclinic space group *Pc*, with four unique complex molecules in their asymmetric unit. These crystals suffered consistently from mild non-merohedral twinning, but a twin law was elucidated which allowed the structure to be fully refined [19]. The unit cell of (R)-**2**·½MeCN (orthorhombic, $P2_12_12_1$) contains two independent molecules of the complex, while the other structures are all more crystallographically routine. Bond lengths and angles within the metal coordination spheres are tabulated in the Supporting Information, and resemble those of other $[Zn(PyBox)_2]^{2+}$ [12, 20] and $[Co(PyBox)_2]^{2+}$ [10, 11] derivatives. Metric parameters from the cobalt complexes are consistent with a high-spin state, as predicted from the magnetic data (Figure 1). This is most evident in the Co–N{pyridyl} bond lengths, which all lie between 2.06-2.09 Å. A low-spin cobalt(II) complex with this ligand geometry would exhibit Co–N{pyridyl} = 1.8-1.9 Å [21].

The geometric distortions caused by intramolecular steric clashes between ligand substituents can be quantified by two parameters: the *trans*-N(pyridyl)–M–N(pyridyl) angle (φ); and the dihedral angle between the least squares planes of the heterocyclic cores of the two ligands (ϑ) [22]. These respectively take values of 180 and 90° in the idealised D_{2d} symmetry for this type of complex (ignoring the PyBox Ph or iPr substituents) but can be significantly reduced in practise, particularly in high-spin complexes [23]. These distortions predominantly reflect the relative dispositions of the two tridentate ligands around the metal ion, rather than significant asymmetry in the metal–ligand bond lengths or ligand bite angles. In the iron compounds in our original study, the steric crowding about the metal ions

was most evident in ϑ, which was close to its ideal value in the heterochiral complexes but consistently reduced in the more congested homochiral congeners (Table 2) [6]. While (R)-**2**, (RS)-**2** and (RS)-**4** exhibit the same crystallographic trend, the L^{Ph} complexes **1** and **3** are less clear-cut, particularly when literature data are also considered (Table 1). However, we can conclude the coordination geometry of $[M(L^{iPr})_2]^{2+}$ (M = Fe, Zn) is more affected by the homochiral or heterochiral nature of the coordinated ligands, than the corresponding $[M(L^{Ph})_2]^{2+}$ derivatives (Figures 2 and 3).

<Insert Figures 2 and 3 and Table 2 here>

Pairs of phenyl substituents in (R)-**1** and (R)-**3**·3MeCN are in close contact with each other, in opposite quadrants of the complex molecule. This has the effect of twisting one phenyl group in each pair, so that one of its C–H groups projects into the face of the pyridyl ring of the other ligand in the molecule. The other phenyl ring in each pair is almost coparallel with its pyridyl ring neighbour, yielding an offset π–π interaction. In (R)-**3**·3MeCN, both stacked and both twisted phenyl rings belong to the same L^{Ph} ligand, giving the molecule approximate C_2 symmetry. This is the conformation found in other crystalline (R)-$[M(L^{Ph})_2]^{2+}$ (M = Fe, Co, Cu, Zn) salts [6, 10-13]. However, in (R)-**1** each L^{Ph} ligand has one stacked and one twisted phenyl group, reducing the approximate molecular symmetry to C_1 (Figure 2). These different substituent conformations imply the phenyl ring orientations exchange in solution, which also explains why all four phenyl rings in (R)-**1** and (R)-**3** are chemically equivalent by NMR (see below). The phenyl rings in (RS)-**1** each occupy a different molecular quadrant and are well separated from each other, leading each of them to adopt a π–π stacked conformation with its co-ligand pyridyl group (Figure 2) [6, 12].

The *iso*propyl substituents in (R)-**2**·½MeCN are oriented to avoid any close steric contact between them, which however leads all four *iso*propyl groups to form close C–H...π contacts with a co-ligand pyridyl or oxazolinyl group. Since these steric repulsions act in two opposite quadrants of the molecule, that accounts for the large ϑ distortion observed in that structure. In (RS)-**2** the *iso*propyl groups have more rotational freedom to minimise their steric impact, and are disposed to exert opposing steric influences on their co-ligands. Hence, ϑ in this isomer is close to its 90° ideal value (Table 1). The same structural trends occur in the corresponding disastereomers of $[Fe(L^{iPr})_2]^{2+}$ [6].

Previous ^{1}H NMR studies have shown that (RS)-$[M(L^{Ph})_2]^{2+}$ (M = Fe, Co or Zn) are stable in solution, and don't undergo racemisation by ligand redistribution [6, 10, 12]. This was also confirmed in the gas phase, by mass spectrometry [9]. Comparison of the ^{1}H NMR spectra of (RS)-**1** and (RS)-**3** with their homochiral congeners confirms that conclusion (Figure 4 and Supporting Information)Figure . There is no evidence for partial decoordination of L^{Ph} in the spectra of the zinc complexes, as was observed for the triflate salt of (R)-**1** under some conditions [12]. That may reflect the lower nucleophilicity of the BF_4^- ion compared to $CF_3SO_3^-$ [24]. Conversely, ^{1}H NMR spectra of pre-formed (RS)-**2** and (RS)-**4** do contain clearly resolved peaks from their homochiral isomers, indicating partial racemisation of those heterochiral complexes (Figure 5 and Supporting Information). The homochiral:heterochiral ratio in these solutions is almost invariant over a 24 hr period, at 1:4 for (RS)-**2** (which is similar to (RS)-$[Fe(L^{iPr})_2]^{2+}$ [6]), and 1:12 for (RS)-**4**. These are lower than the statistical ratio

of 1:1, implying that the reduced steric crowding in the heterochiral isomer does make some contribution to its stability.

<center><Insert Figures 4 and 5 here></center>

The solution structures of the diastereomers of **1** were also probed with NOESY spectra. The main difference between the two isomers is that the *meta* phenyl $H^{3/5}$ protons exhibit strong NOEs with only one of the diastereotopic oxazolyl H^5 environments in (R)-**1**, but show NOEs with both these H atoms in (RS)-**1**. That is consistent with the crystallographic structures of those compounds, where the same *meta* proton in each phenyl ring of (RS)-**1** lies close to the oxazolyl *endo*-H^5 proton in the same ligand, and to the *exo*-H^5 proton in the co-ligand (Figure 2). In contrast, the phenyl rings in (R)-**1** each lie close to the oxazolyl *endo*-H^5 environment in both ligands, so only one NOE is observed in that isomer. A similar analysis was also attempted for **2**, but NOEs to the overlapping oxazolyl H^5 proton environments in (RS)-**2** could not be distinguished in that isomer. Interestingly the phenyl rings in each isomer of **1** and **3** are all C_2-symmetric by NMR, which is inconsistent with the crystallographic L^{Ph} ligand environments and implies rapid rotation of the phenyl rings. The *iso*propyl groups in **2** and **4** are diastereotopic by NMR, as expected, but this gives no information about their conformational flexibility.

4. Conclusion

Our recent study of the diastereomers of $[Fe(L^{Ph})_2]^{2+}$ and $[Fe(L^{iPr})_2]^{2+}$ [6] has been extended to the corresponding cobalt(II) and zinc(II) complexes. Our results confirm that (RS)-$[M(L^{Ph})_2]^{2+}$ (M = Fe [6], Co [10] and Zn [12]) does not racemise through ligand redistribution reactions in solution, but that (RS)-$[M(L^{iPr})_2]^{2+}$ does partially racemise. Since (RS)-$[Co(L^{Me})_2]^{2+}$ and (RS)-$[Co(L^{Bn})_2]^{2+}$ also undergo racemisation in solution [10], it appears the stability of (RS)-$[M(L^{Ph})_2]^{2+}$ does not reflect the steric properties of the L^{Ph} phenyl substituents, but is a unique property of the (RS)-$[M(L^{Ph})_2]^{2+}$ centre itself.

The substoichiometric ratio of diastereomers in solutions of (RS)-**2** and (RS)-**4** implies that the more distorted molecular structure in (R)-$[M(L^{iPr})_2]^{2+}$ (M = Fe, Co or Zn) has an influence on the relative stability of the two isomers. However, the stabilisation of (RS)-$[M(L^{Ph})_2]^{2+}$ over (R)-$[M(L^{Ph})_2]^{2+}$ cannot reflect their coordination geometries, since the larger sterically-imposed geometry distortion in (R)-$[M(L^{iPr})_2]^{2+}$ does not prevent racemisation. Rather, the additional stability of (RS)-$[M(L^{Ph})_2]^{2+}$ could arise from its four intramolecular $\pi...\pi$-interactions, whereby each L^{Ph} pyridyl ring is sandwiched between the two phenyl substituents of the other L^{Ph} ligand (Figure 2). These $\pi...\pi$-interactions are disrupted in homochiral (R)-$[M(L^{Ph})_2]^{2+}$ because of steric clashes between phenyl rings, which may slightly destabilise the homochiral isomer of that complex.

Acknowledgments

Appendix A. Supplementary data

CCDC- 1830132-1830137 contain the supplementary crystallographic data for this paper. These data can be obtained free of charge via http://www.ccdc.cam.ac.uk/conts/retrieving.html, or from the Cambridge Crystallographic Data Centre, 12 Union Road, Cambridge CB2 1EZ, UK; fax: (+44) 1223-336-033; or e-mail: deposit@ccdc.cam.ac.uk. Supplementary information associated with this article can be found, in the online version, at http://dx.doi.org/10.1016/j.poly.####.

Data supporting this study are available at http://doi.org/10.5518/###.

References

[1] M. K. Tse, S. Bhor, M. Klawonn, G. Anilkumar, H. Jiao, C. Döbler, A. Spannenberg, W. Mägerlein, H. Hugl, M. Beller, Chem. Eur. J. 12 (2006) 1855.

[2] a) J. S. Johnson, D. A. Evans, Acc. Chem. Res. 33 (2000) 325;

b) G. Desimoni, G. Faita, P. Quadrelli, Chem. Rev. 103 (2003) 3119;

c) S. Kobayashi, Y. Yamashita, Acc. Chem. Res. 44 (2011) 58;

d) B. D. Ward, L. H. Gade, Chem. Commun. 48 (2012) 10587;

e) G. Bauer, X. Hu, Inorg. Chem. Front. 3 (2016) 741.

[3] a) S. Chorazy, K. Nakabayashi, K. Imoto, J. Mlynarski, B. Sieklucka, S. Ohkoshi, J. Am. Chem. Soc. 134 (2012) 16151;

b) S. Chorazy, K. Nakabayashi, N. Ozaki, R. Pelka, T. Fic, J. Mlynarski, B. Sieklucka, S. Ohkoshi, RSC Adv. 3 (2013) 1065;

c) S. Chorazy, K. Nakabayashi, M. Arczynski, R. Pelka, S. Ohkoshi, B. Sieklucka, Chem. Eur. J. 20 (2014) 7144.

[4] T. Y. Bing, T. Kawai, J. Yuasa, J. Am. Chem. Soc. 140 (2018) 3683.

[5] a) Y. Y. Zhu, C. W. Liu, J. Yin, Z. S. Meng, Q. Yang, J. Wang, T. Liu, S. Gao, Dalton Trans. 44 (2015) 20906;

b) Y.-Y. Zhu, H.-Q. Li, Z.-Y. Ding, X.-J. Lü, L. Zhao, Y.-S. Meng, T. Liu, S. Gao, Inorg. Chem. Front. 3 (2016) 1624;

c) A. Kimura, T. Ishida, Inorganics 5 (2017) 52.

[6] K. E. Burrows, S. E. McGrath, R. Kulmaczewski, O. Cespedes, S. A. Barrett, M. A. Halcrow, Chem. Eur. J. 23 (2017) 9067.

[7] L. J. Kershaw Cook, R. Mohammed, G. Sherborne, T. D. Roberts, S. Alvarez, M. A. Halcrow, Coord. Chem. Rev. 289-290 (2015) 2.

[8] Chiral discrimination of spin-crossover has also been observed in the solid state, either between optical isomers of the same material or through diastereomeric solvent inclusion. However these phenomena reflect differences in crystallographic symmetry and/or extended lattice effects, as well as more subtle influences of chirality on the molecular ligand field. See ref [6], and:
a) Q. Wang, S. Venneri, N. Zarrabi, H. Wang, C. Desplanches, J.-F. Létard, T. Seda, M. Pilkington, Dalton Trans. 44 (2015) 6711;

b) I. A. Gural'skiy, O. I. Kucheriv, S. I. Shylin, V. Ksenofontov, R. A. Polunin, I. O. Fritsky, Chem. Eur. J. 21 (2015) 18076;

c) L.-F. Qin, C.-Y. Pang, W.-K. Han, F.-L. Zhang, L. Tian, Z.-G. Gu, X. Ren, Z. Li, CrystEngComm 17 (2015) 7956;

d) L.-F. Qin, C.-Y. Pang, W.-K. Han, F.-L. Zhang, L. Tian, Z.-G. Gu, X. Ren, Z. Li, Dalton Trans. 45 (2016) 7340;

e) Y. Sekimoto, M. R. Karim, N. Saigo, R. Ohtani, M. Nakamura, S. Hayami, Eur. J. Inorg. Chem. (2017) 1049.

[9]   H. Sato, Y. Suzuki, Y. Takai, H. Kawasaki, R. Arakawa, M. Shizuma, Chem. Lett. 39 (2010) 564.

[10] C. Provent, G. Bernardinelli, A. F. Williams, N. Vulliermet, Eur. J. Inorg. Chem. (2001) 1963.

[11] J. Guo, B. Wang, J. Bi, C. Zhang, H. Zhang, C. Bai, Y. Hu, X. Zhang, Polymer 59 (2015) 124.

[12] S. Saaby, K. Nakama, M. A. Lie, R. G. Hazell, K. A. Jørgensen, Chem. Eur. J. 9 (2003) 6145.

[13] D. A. Evans, M. C. Kozlowski, J. A. Murry, C. S. Burgey, K. R. Campos, B. T. Connell, R. J. Staples, J. Am. Chem. Soc. 121 (1999) 669.

[14] C. J. O'Connor, Prog. Inorg. Chem. 29 (1982) 203.

[15] a) D. F. Evans, J. Chem. Soc. (1959) 2003;

b) E. M. Schubert, J. Chem. Educ. 69 (1992) 62.

[16] B. García, J. C. Ortega, J. Chem. Eng. Data 33 (1988) 200.

[17] G. M. Sheldrick, Acta Cryst. Sect. C.: Struct. Chem. 71 (2015) 3.

[18] O. V. Dolomanov, L. J. Bourhis, R. J. Gildea, J. A. K. Howard, H. Puschmann, J. Appl. Cryst. 42 (2009) 339.

[19] Crystals of (*RS*)-**3**·2.5MeCN were isostructural with (*RS*)-**1**·2.5MeCN and suffered from the same non-merohedral twinning, but diffracted more weakly and could not be refined satisfactorily. Unit cell data for (*RS*)-**3**·2.5MeCN: $C_{51}H_{45}B_2CoF_8N_{8.5}O_4$, M_r = 1074.02, monoclinic, *Pc*, a = 21.2183(3), b = 22.4547(5), c = 20.7183(3) Å, β = 91.6703(12)°, V = 9867.1(3) Å^3.

[20] a) M. Jiang, S. Dalgarno, C. A. Kilner, M. A. Halcrow, T. P. Kee, Polyhedron 20 (2001) 2151;

b) H.-Q. Li, Z.-Y. Ding, Y. Pan, C.-H. Liu, Y.-Y. Zhu, Inorg. Chem. Front. 3 (2016) 1363.

[21] See *eg*

   a) B. N. Figgis, E. S. Kucharski, A. H. White, Aust. J. Chem. 36 (1983) 1537;

   b) A. Galet, A. B. Gaspar, M. C. Muñoz, J. A. Real, Inorg. Chem. 45 (2006) 4413;

   c) C. A. Kilner, M. A. Halcrow, Dalton Trans. 39 (2010) 9008;

   d) J. Palion-Gazda, B. Machura, R. Kruszynski, T. Grancha, N. Moliner, F. Lloret, M. Julve, Inorg. Chem. 56 (2017) 6281.

[22] J. M. Holland, J. A. McAllister, C. A. Kilner, M. Thornton-Pett, A. J. Bridgeman, M. A. Halcrow, J. Chem. Soc. Dalton Trans. (2002) 548.

[23] M. A. Halcrow, Coord. Chem. Rev. 253 (2009) 2493.

[24] W. Linert, R. F. Jameson, A. Taha, J. Chem. Soc. Dalton Trans. (1993) 3181.

Table 1. Experimental details for the single crystal structure determinations in this work. All data were collected using Cu-K_α radiation (λ = 1.5418 Å), unless otherwise stated.

	(R)-1	(RS)-1·2.5MeCN	(R)-2·0.5MeCN	(RS)-2
Formula	$C_{46}H_{38}B_2F_8N_6O_4Zn$	$C_{51}H_{45}B_2F_8N_{8.5}O_4Zn$	$C_{35}H_{47.5}B_2F_8N_{6.5}O_4Zn$	$C_{34}H_{46}B_2F_8N_6O_4Zn$
M_r	977.81	1312.94	862.28	841.76
Crystal system	monoclinic	monoclinic	orthorhombic	monoclinic
Space group	$P2_1$	Pc	$P2_12_12_1$	$P2_1/n$
a (Å)	11.1726(2)	21.2573(2)	12.6116(1)	9.1655(1)
b (Å)	16.6498(3)	22.4616(2)	15.3947(2)	23.1136(2)
c (Å)	12.4526(3)	20.7784(2)	40.6472(4)	17.7795(1)
α (°)	–	–	–	–
β (°)	111.610(2)	91.4956(9)	–	95.7046(8)
γ (°)	–	–	–	–
V (Å³)	2153.64(8)	9917.72(17)	7891.73(14)	3747.71(5)
Z	2	8	8	4
T (K)	120(2)	120(2)	120(2)	120(2)
D_{calc} (g.cm⁻³)	1.508	1.432	1.452	1.492
μ (mm⁻¹)	1.557	1.417	1.609	1.675
Measured, independent reflections	17464, 8122	97837, 34777	34841, 15076	34739, 7398
R_{int}	0.029	0.048	0.035	0.029
Observed reflections [$I > 2\sigma(I)$]	7904	31148	14069	6927
Data, restraints, parameters	8122, 109, 604	34777, 58, 2725	15076, 0, 1053	7398, 0, 504
$R_1(I > 2\sigma(I))$[a], wR_2(all data)[b]	0.033, 0.080	0.091, 0.285	0.037, 0.089	0.029, 0.073
GOF	1.081	1.268	1.028	1.033
$\Delta\rho_{min}$, $\Delta\rho_{max}$ (e.Å⁻³)	−0.26, 0.32	−0.96, 3.12	−0.49, 0.98	−0.34, 0.55
Flack parameter	−0.022(10)	0.00(5)	−0.002(10)	–

Table 1 (continued)

	(R)-**3**·3MeCN	(RS)-**4**·MeCN
Formula	$C_{52}H_{47}B_2CoF_8N_9O_4$	$C_{36}H_{49}B_2CoF_8N_7O_4$
M_r	1094.53	876.37
Crystal system	monoclinic	triclinic
Space group	$P2_1$	$P\bar{1}$
a (Å)	10.8167(1)	11.7604(2)
b (Å)	21.3675(2)	11.8654(2)
c (Å)	11.7629(1)	16.0917(2)
α (°)	–	76.435(1)
β (°)	112.513(1)	85.973(1)
γ (°)	–	89.895(1)
V (Å³)	2511.54(5)	2177.19(6)
Z	2	2
T (K)	120(2)	100(2)
D_{calc} (g.cm⁻³)	1.447	1.337
μ (mm⁻¹)	3.420	0.438[c]
Measured, independent reflections	19234, 9866	22384, 8537
R_{int}	0.028	0.042
Observed reflections [$I > 2\sigma(I)$]	9536	7652
Data, restraints, parameters	9866, 1, 688	8537, 44, 547
$R_1(I > 2\sigma(I))$[a], wR_2(all data)[b]	0.031, 0.077	0.074, 0.227
GOF	1.003	1.061
$\Delta\rho_{min}$, $\Delta\rho_{max}$ (e.Å⁻³)	−0.28, 0.62	−0.65, 1.08
Flack parameter	−0.0208(12)	–

[a]$R = \Sigma [|F_o| - |F_c|] / \Sigma |F_o|$ [b]$wR = [\Sigma w(F_o^2 - F_c^2) / \Sigma wF_o^4]^{1/2}$ [c]collected using synchrotron radiation.

Table 2. Coordination geometry distortion parameters for the compounds in this work. Selected literature data are also included for comparison. The iron and cobalt complexes are high-spin unless otherwise noted.

	φ	ϑ	Ref
(R)-**1**	171.21(13)	85.28(3)	This work
(RS)-**1**·2.5MeCN[a]	171.63(19)–177.1(2)	88.24(7)–89.91(7)	This work
(R)-[Zn(L^{Ph})$_2$][Tf]$_2$·CH$_2$Cl$_2$	176.4	86.6	[12]
(RS)-[Zn(L^{Ph})$_2$][Tf]$_2$·2CH$_2$Cl$_2$	180	88.3	[12]
(R)-**2**·½MeCN[b]	163.59(12)–171.97(12)	70.30(2)–70.41(2)	This work
(RS)-**2**	162.15(4)	89.39(1)	This work
(R)-**3**·3MeCN	171.36(9)	83.62(2)	This work
(R)-[Co(L^{Ph})$_2$][ClO$_4$]$_2$·3MeCN	171.7	84.1	[10]
(R)-[Co(L^{Ph})$_2$][CoCl$_4$]$_2$·2dmf	176.1	89.5	[11]
(RS)-**4**·MeCN	172.20(10)	89.96(3)	This work
(R)-[Fe(L^{Ph})$_2$][ClO$_4$]$_2$·MeCN[c,d]	177.75(10)–179.51(9)	82.45(2)–86.00(2)	[6]
(RS)-[Fe(L^{Ph})$_2$][ClO$_4$]$_2$·3MeCN[d]	178.18(8)	88.94(2)	[6]
(R)-[Fe(L^{iPr})$_2$][ClO$_4$]$_2$·½MeCN[b]	165.50(12)–175.44(11)	70.03(3)–70.32(3)	[6]
(RS)-[Fe(L^{iPr})$_2$][ClO$_4$]$_2$	163.62(6)	89.23(1)	[6]

[a]There are four crystallographically unique cations in this crystal structure. [b]There are two unique cations in this crystal structure. [c]There are three unique cations in this crystal structure. [d]This complex is low-spin at the temperature of measurement.
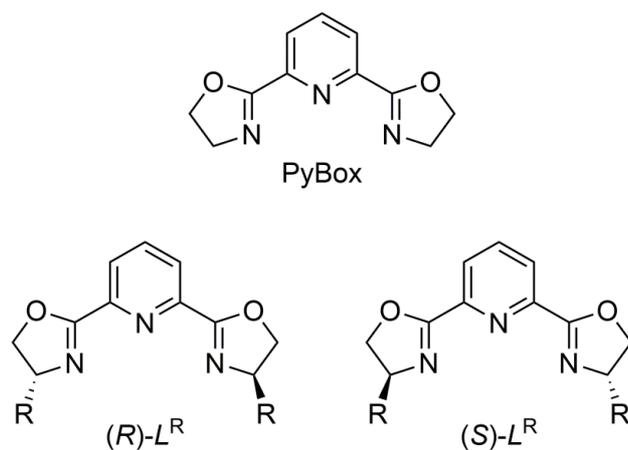
Scheme 1. The ligands referred to in this work (R = Me, Ph, ^{i}Pr or Bn).
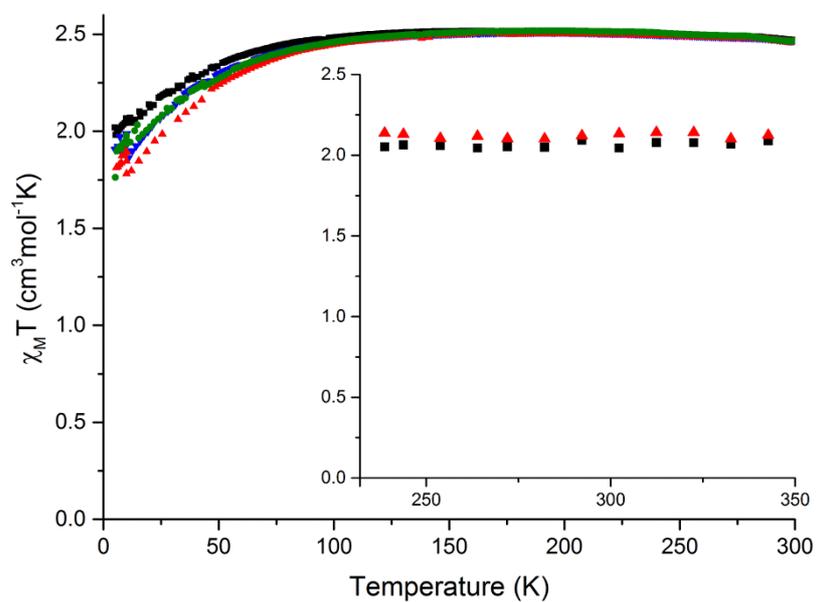
Figure 1. Solid state magnetic susceptibility data for (*R*)-**3** (black squares), (*RS*)-**3** (red triangles), (*R*)-**4** (blue triangles) and (*RS*)-**4** (green circles). Inset: solution phase magnetic data for (*R*)-**3** and (*RS*)-**3** in CD$_3$CN.
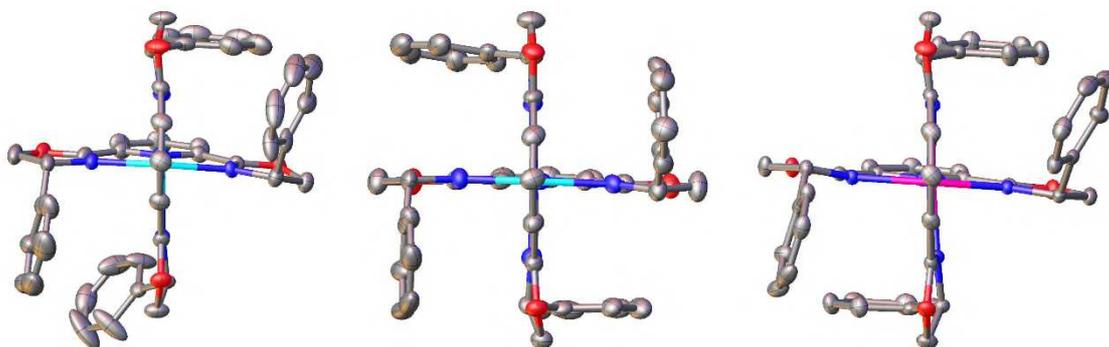
Figure 2. Complex dications in the crystal structures of (*R*)-**1** (left), (*RS*)-**1** (molecule A; centre) and (*R*)-**3** (right). Only one orientation of the disordered phenyl substituents in (*R*)-**1** is shown. Displacement ellipsoids are at the 50 % probability level, and hydrogen atoms are omitted for clarity. Colour code: C, grey; Co, pink; N, blue; O, red; Zn, cyan.
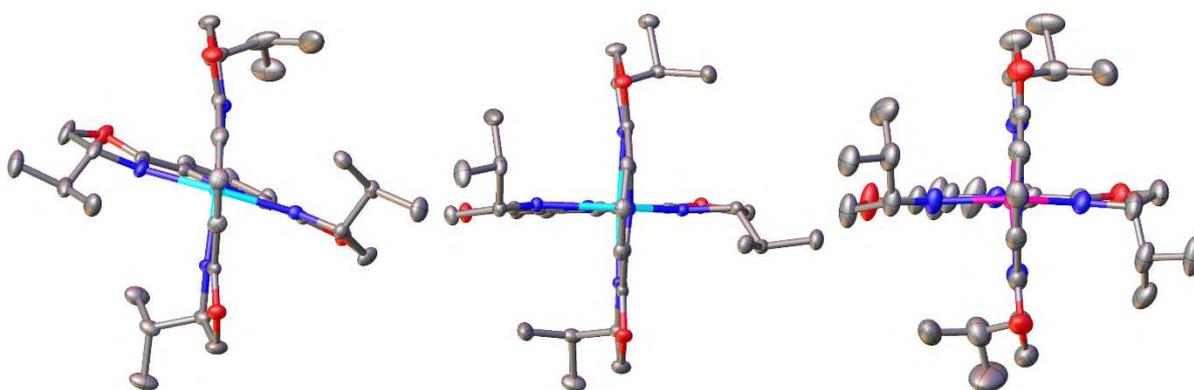
Figure 3. Complex dications in the crystal structures of (*R*)-**2** (molecule A; left), (*RS*)-**2** (centre) and (*RS*)-**4** (right). Details as for Figure 2.
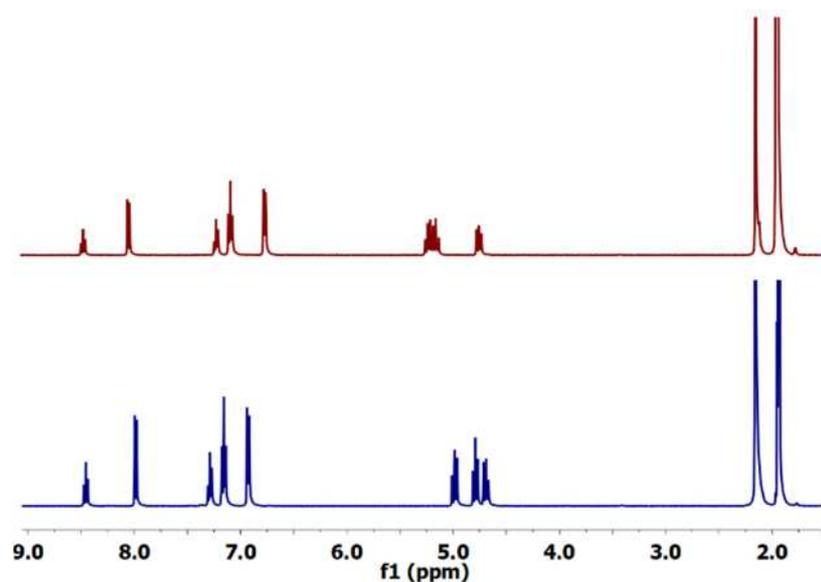
Figure 4. ^{1}H NMR spectra (CD$_3$CN) of (*R*)-**1** (red, top) and (*RS*)-**1** (blue, bottom). There is no evidence for the homochiral isomer in the spectrum of (*RS*)-**1**, which would indicate racemisation of the complex in solution. ^{1}H NMR spectra of (*R*)-**3** and (*RS*)-**3** are shown in the Supporting Information.
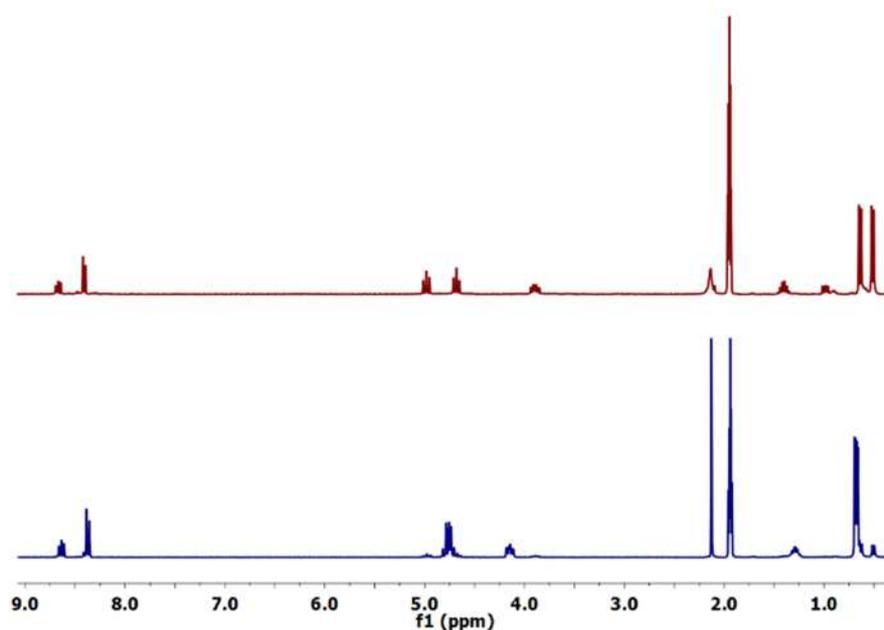
Figure 5. ^{1}H NMR spectra (CD$_3$CN) of (*R*)-**2** (red, top) and (*RS*)-**2** (blue, bottom), which also contains a small population of the homochiral isomer. ^{1}H NMR spectra of (*R*)-**4** and (*RS*)-**4** are shown in the Supporting Information.